Operational modal analysis of an eight-storey building with asynchronous data incorporating multiple setups

Yi-Chen Zhu[1], Yan-Long Xie[2] and Siu-Kui Au[3]

Institute for Risk and Uncertainty and Centre for Engineering Dynamics

University of Liverpool, United Kingdom

Abstract

This paper presents operational modal analysis of an eight-storey concrete building using ambient vibration data collected in an 'asynchronous' manner, i.e., different sensors using possibly different clocks for data sampling. Five force-balance accelerometers were used with a number of setups to cover all locations of interests. Modal identification is performed using a Bayesian frequency domain method for asynchronous data and the global mode shape is assembled using the global least square method. The identified modal parameters based on asynchronous data are evaluated by comparing with those identified based on synchronous data. The identification uncertainties of modal parameters are investigated through the posterior coefficient of variation in a Bayesian context. The study provides insights into the challenges encountered when using asynchronous data for operational modal analysis in a practical context.

Key Words: Asynchronous data; Bayesian methods; Full-scale tests; Operational modal analysis

1. Introduction

Structural health monitoring (SHM) has the general objective of monitoring the physical conditions of structures with potential applications in detecting damage during their service

[1] Corresponding author. Harrison Hughes Building, Brownlow Hill, Liverpool, L69 3GH, UK. Email: sgyzhu7@liverpool.ac.uk.
[2] Email: yanlong.xie@liverpool.ac.uk
[3] Email: siukuiau@liverpool.ac.uk

life [1–5]. Various means for SHM have been proposed in the past few decades by measuring structural response such as strain, displacement and acceleration. Modal identification aims at identifying the modal properties involving natural frequencies, damping ratios and mode shapes based on the measured structural response data. It is often the first step in SHM that provides the baseline information on the current state of the subject structure [6–9].

For civil infrastructures which are typically large-scale, operational modal analysis (OMA), also known as ambient modal identification, has been widely used. It can be conducted when the structure is under environmental excitations such as wind, cultural activities and microtremor without artificial loading conditions. In OMA, the excitation is unknown but assumed to be 'broadband random'. Due to its high economy and feasibility, OMA has attracted great attention in both theory development and real applications in recent years [10–12]. It provides important information for downstream applications such as finite element model updating [13–17].

In full-scale tests, mode shape information is often demanded where the vibration response at multiple locations needs to be measured. Due to the limited number of instruments or difficulties in their deployment, it often happens that the interested DOFs (degrees of freedom) cannot be all measured in a single setup. In this case, a common strategy is to conduct multiple setups covering different DOFs in each setup with some reference DOFs in common [18–22]. Conventionally, the modal parameters in individual setups are identified separately using single-setup modal identification methods and the global mode shape is assembled from the local ones identified in different setups. Assembly techniques have been developed where the global mode shape is determined as the one that minimises the discrepancies between local mode shapes in different setups in a least square sense [23,24]. OMA method incorporating multiple setups have also been developed in both non-Bayesian [25] and Bayesian [26] context. Multiple-setup algorithms have also been applied to structural modal updating [27,28].

Time synchronisation is another issue which should be considered in real implementations. Conventional OMA approaches assume that the digital data from different channels in each setup are synchronised, i.e., sampled based on the same time scale. Simply recording the data from multiple channels with the same duration does not imply that they are synchronised. The sampling pace in different sensors needs to be real-time controlled by a synchronisation protocol. Transmitting analogue data from sensors directly to a central synchronisation

console requires long cables, with implications on logistics, voltage drop and noise. Alternative options exist, e.g., Network Time Protocol [29], Global Positioning System [30] and wireless sensor networks [31–33], requiring varying degrees of communication infrasture on site. If modal identification can be performed for asynchronous data, field tests can be conducted in a more economical and flexible manner compared to synchronous data. However, lower identification quality is expected because less information is available.

This paper investigates the quality of modal identification results based on asynchronous ambient data incorporating multiple setups in full-scale tests. An eight-storey concrete building is used as a vehicle for investigation, where complication and practical aspects in field implementation are naturally reflected in the data. Bayesian OMA methods assuming synchronous [34] or asynchronous data [35,36] are applied to the data of each setup individually. The global mode shape is assembled from the most probable local mode shapes in individual setups based on the global least square method [23]. The quality of identified modal parameters based on asynchronous data is compared against their synchronous counterpart. In addition to the most probable value, identification uncertainties associated with the modal parameters are also discussed for both synchronous and asynchronous cases. This work provides an opportunity to investigate the effect of asynchronous data in OMA under full-scale test configurations. Practical issues with time synchronisation and challenges encountered in real applications are also discussed.

This paper is organised as follow. The basic properties of the tested building are presented in Section 2. Section 3 provides detailed information about the field instrumentation. The modal identification methods used in this work are briefly reviewed in Section 4. The identification results and posterior uncertainties are investigated in Section 5. The work is concluded in Section 6.

2. Description of field structure

Brodie Tower is a reinforced-concrete building situated on the campus of the University of Liverpool (Figure 1). It has eight storeys with a total height of approximately 25m. The ground floor of the building is connected to another office building (Muspratt Building, see Figure 1). From 1/F to 7/F, the floor slabs are T-shaped spanning over a $25\text{m} \times 28\text{m}$ area; see Figure 2, where sensor locations are discussed later in Section 3.2. The ground floor of the

building is used as a social space and the remaining floors are mainly office and lecture rooms.

Figure 1. Brodie Tower

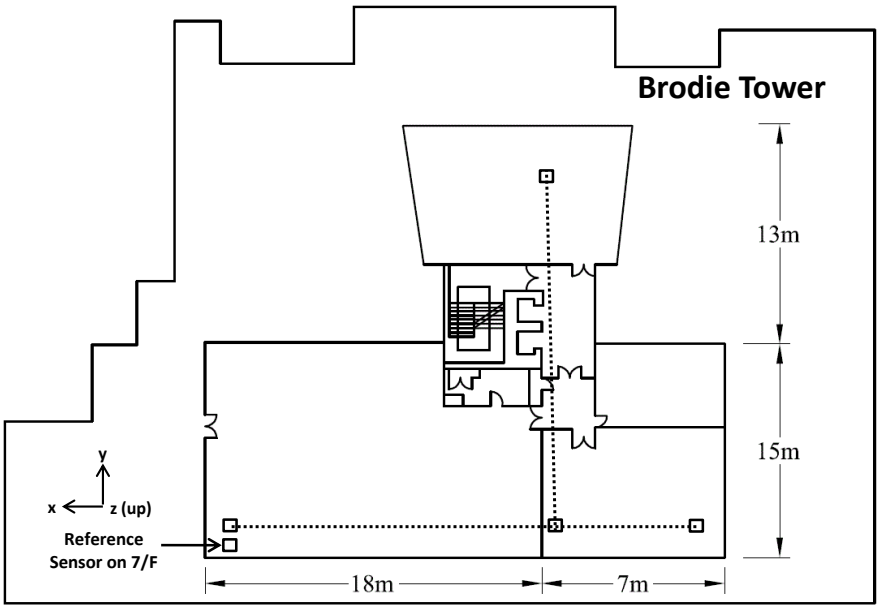

Figure 2. Floor Plan with Sensor Locations

3. Instrumentation

Five force-balance triaxial accelerometers were deployed to measure the ambient vibration of the structure. The equipment for each sensor location comprises accelerometer, GPS receiver,

high-precision clock, battery and accessories (e.g., cables). These are hosted in a water-proof rugged case in-house designed for mobile field deployment, see Figure 3.

Analogue voltage signals of acceleration were acquired by a 24-bit data logger at a sampling rate of 50Hz. The noise level of the accelerometers is about $0.1\mu g/\sqrt{Hz}$ in the frequency band above 1Hz. In each setup, the acceleration data comprises $5\times3=15$ channels for twenty minutes.

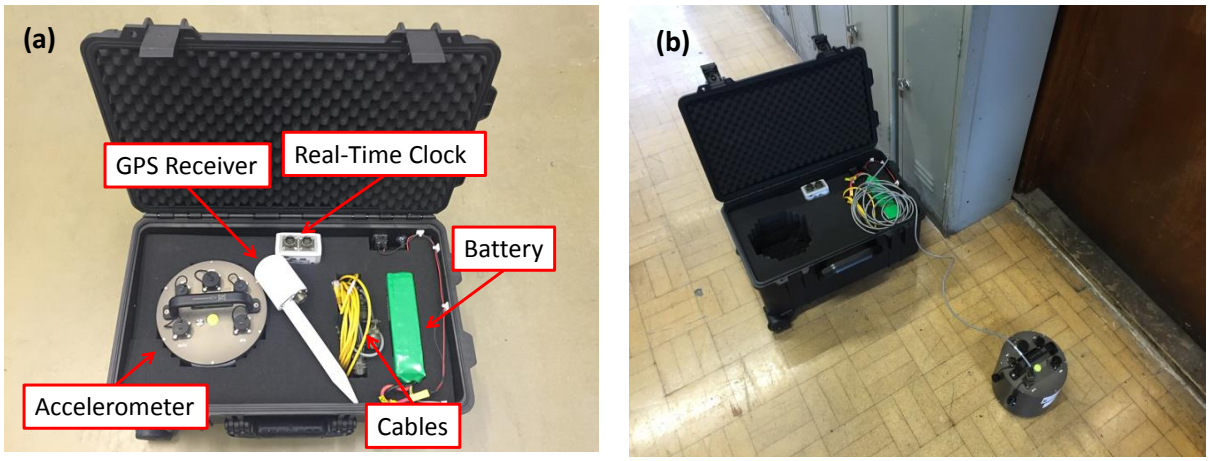

Figure 3. Equipment per Sensor Location (a) Instrument (b) On-Site View

3.1 Sensor locations

In view of the floor plan in Figure 2, it was intended to obtain a mode shape that resolves into the 'T-shape'. Compromising with the available number of sensors, four locations on each floor from 1/F to 7/F with one reference location on 7/F were measured, giving $(4\times7+1)\times3=87$ degrees of freedom (DOFs) in total. For feasibility and convenience in alignment, the sensors were located in the corridors and they were oriented along the frame direction of the building.

3.2 Reference sensor

Due to the limited number of sensors, only 5 locations (15 DOFs) can be measured in a single setup. Multiple setups are thus necessary to cover all the 29 locations (87 DOFs) of interest. The mode shapes identified in different setups are under different scaling and it is necessary for different setups to share some 'reference DOFs' so that their 'local mode shapes' can be assembled into a 'global mode shape' comprising the DOFs measured in all setups. The data at the reference DOFs should contain significant responses of all the modes of interest (i.e., avoid nodal locations). In this test, one reference sensor was placed in all setups on 7/F near

the lower left cover of Figure 2. That location was expected to have significant vibration response and was unlikely to be a node.

3.3 Roving setups

To cover the DOFs in Figure 2, the remaining four sensors were ‘roved’ to different floors in different setups, leading to seven setups. In order to investigate the effect of imperfect synchronisation on modal identification, ideally it would be desirable to have two sets of data, one synchronous and the other asynchronous, during exactly the same time period. Due to the limited number of sensors and the impossibility of placing two sensors at exactly the same location, this was not feasible, however. As a practical alternative, asynchronous data was collected first, followed by synchronous data.

The setups for asynchronous data were conducted (i.e., each sensor sampled the data using its own clock) in the morning from 8:30 to 12:30 in the order of 7/F to 4/F, 2/F, 3/F and 1/F. The setup on 3/F was conducted after the one on 2/F as there was an examination in the lecture room on 3/F at that time. After the setups for asynchronous data, all the sensors were synchronised using ‘real-time’ clocks (see details in Section 3.4). The setups for synchronous data were then conducted in the afternoon from 14:30 to 17:10 with the order from 7/F to 1/F. Figure 4 shows a schematic diagram of the setup plans and the measured DOFs of Setup 3 (i.e., 5/F) for synchronous data.

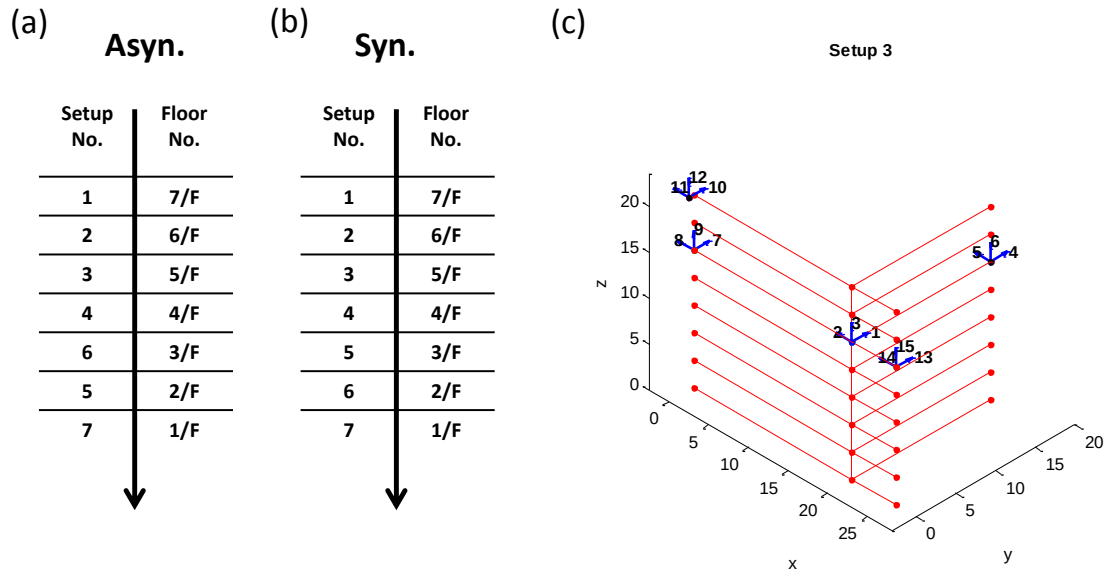

Figure 4. Schematic Diagram of Setup Plans for (a) Asynchronous Data Set (b) Synchronous Data Set (c) Measured DOFs of Setup 3 for Synchronous Data Set

During the test, two participants were involved, each responsible for two sensors. The transition between setups typically took five minutes, including levelling and alignment. For both synchronous and asynchronous data, the sensors were controlled to start measuring at the same time with twenty five minutes duration for each setup, allowing five minutes as a buffer.

3.4 Time synchronisation

In this work, the asynchronous data are obtained by simply logging the data locally for each sensor. That is, each sensor uses its own clock to sample the data and the clocks in different sensors are not synchronised. For synchronous data, as most of the locations in this test were indoor and GPS signal was weak, it was not possible to synchronise different sensors using GPS. 'Real-time' clocks were used for time synchronisation in this test. These are high-precision clocks producing data that can be considered as practically synchronous when the frequency of interest is not too high and the data duration is not too extended. The clocks were first synchronised and trained using GPS receivers. Once the clocks were locked, the GPS receivers were disconnected and the clocks run independently. The real-time clocks used in this test have an accuracy of 0.038ppm (parts per million). This corresponds to a relative drift of $2\times 0.038\times 10^{-6}\times 3600\times 12\approx 3\text{ms}$ over 12 hours. For the frequency range of interest $\ll 1/3\times 10^{-3}\approx 300\text{Hz}$, the data can be considered as practically synchronised.

4. Modal identification methods

To investigate the effect of asynchronous data on the quality of modal identification results, a Bayesian frequency-domain approach is used to identify the modal properties of the instrumented structure and quantify identification uncertainties based on the measured ambient data. Bayesian approach provides a fundamental way to identify the modal parameters, where physical modelling assumptions are obeyed and information in the measured data is fully used for making inference about the modal parameters. In addition to the most probable values (MPV) of modal parameters, it can also quantify identification uncertainties through the posterior covariance matrix. The original formulation was applicable for synchronous data in a single setup and was first proposed in [37]. Fast algorithms have been developed that allow practical implementation in different contexts, e.g., well-separated modes, multiple modes and multiple setups [38]. In this work, for synchronous data, the MPV of modal parameters and posterior uncertainties are determined using [34]. On the other hand, the asychornous conterparts are determined using [35,36]. To assemble the global mode shape from the ones identified in individual setups, a global least-square method [23] is used. In this section, the methods used are briefly reviewed.

4.1 Bayesian frequency domain methods

Let $\left\{\hat{\ddot{\mathbf{x}}}_j \in R^n\right\}_{j=1}^N$ be the measured ambient vibration data at n DOFs, where N is the number of samples per channel. It is modelled to consist of the theoretical structural response $\ddot{\mathbf{x}}_j \in R^n$ under ambient excitation and prediction error $\boldsymbol{\varepsilon}_j \in R^n$:

$$\hat{\ddot{\mathbf{x}}}_j = \ddot{\mathbf{x}}_j + \boldsymbol{\varepsilon}_j \tag{1}$$

The prediction error accounts for the discrepancy between the theoretical model and measured data, which may arise from measurement noise or modelling error. The (scaled) Fast Fourier Transform (FFT) of $\left\{\hat{\ddot{\mathbf{x}}}_j\right\}$ is defined as:

$$\mathcal{F}_k = \sqrt{\frac{2\Delta t}{N}} \sum_{j=1}^{N} \hat{\ddot{\mathbf{x}}}_j \exp\left[-2\pi \mathbf{i} \frac{(k-1)(j-1)}{N}\right] \tag{2}$$

where $\mathbf{i}^2 = -1$ and Δt is the sampling interval; $k = 1,..., N_q \left(N_q = \text{int}\left(N/2\right)+1\right)$ is the index corresponding to the Nyquist frequency N_q and int(.) denotes the integral part of its argument. The scaling factor is $\sqrt{2\Delta t / N}$ such that the PSD is one-sided with respect to

frequency in Hz. For modal identification, only the $\mathcal{F}_k$ within a selected frequency band dominated by the modes of interested is used. Let $\{\mathcal{F}_k\}$ denote such collection of $\mathcal{F}_k$. Using Bayes' theorem and assuming a uniform prior PDF, the posterior PDF of the set of modal parameters $\boldsymbol{\theta}$ given $\{\mathcal{F}_k\}$ is proportional to the likelihood function, i.e. $p(\boldsymbol{\theta}|\{\mathcal{F}_k\}) \propto p(\{\mathcal{F}_k\}|\boldsymbol{\theta})$. For small Δt (i.e., high sampling rate) and large $N\Delta t$ (i.e., long data duration) which is often met in real applications, $\{\mathcal{F}_k\}$ are asymptotically independent at different frequencies and jointly 'circularly complex Gaussian' [39]. The likelihood function is then given by:

$$p(\{\mathcal{F}_k\}|\boldsymbol{\theta}) = (\pi)^{-nN_f} \times \prod_k (\det \mathbf{E}_k)^{-1} \exp\left[-\sum_k \mathcal{F}_k^* \mathbf{E}_k^{-1} \mathcal{F}_k\right] \tag{3}$$

where '*' denotes conjugate transpose; $\mathbf{E}_k$ is the theoretical covariance matrix of $\mathcal{F}_k$ and N_f is the number of FFT data in the selected frequency band. For analysis and computation, it is more convenient to write the likelihood function in a logarithmic form, i.e., the 'negative log-likelihood function' (NLLF)

$$L(\boldsymbol{\theta}) = \sum_k \ln \det \mathbf{E}_k + \sum_k \mathcal{F}_k^* \mathbf{E}_k^{-1} \mathcal{F}_k \tag{4}$$

such that $p(\boldsymbol{\theta}|\{\mathcal{F}_k\}) \propto \exp[-L(\boldsymbol{\theta})]$. With sufficient data, modal identification problem is 'globally identifiable' [40]. The MPV of $\boldsymbol{\theta}$ is then the one that maximises the posterior PDF, or equivalently minimises the NLLF. The identification uncertainty can be fully characterised by the posterior covariance matrix, or equivalently the inverse of Hessian of the NLLF. In this work, the identification uncertainty of a particular modal parameter is discussed based on the posterior coefficient of variation (c.o.v.), which is equal to the ratio of its standard deviation to its MPV. The standard deviation is given by the square root of the corresponding diagonal element of the posterior covariance matrix. The posterior c.o.v. of mode shape is given by the square root sum of the eigenvalues of their posterior covariance matrix. The latter can be obtained from the corresponding partition in the full posterior covariance matrixof all modal parameters. See [41] for details.

Bayesian method for synchronous data

Determining the MPV of modal parameters requires numerical minimisation of the NLLF. In this work, the modes studied are well-separated and such algorithm is presented. In this case, the set of modal parameters consists of the natural frequency f, damping ratio ζ, mode

shape $\boldsymbol{\varphi}$ ($\|\boldsymbol{\varphi}\|=1$), modal force PSD S and prediction error PSD S_e. The FFT of measured acceleration data can then be modelled as

$$\mathcal{F}_k = \boldsymbol{\varphi}\ddot{\eta}_k + \boldsymbol{\varepsilon}_k \tag{5}$$

where $\ddot{\eta}_k$ denotes the FFT of modal acceleration $\ddot{\eta}(t)$ and $\boldsymbol{\varepsilon}_k$ is the scaled FFT of measurement noise. Assuming classically damped structure, $\ddot{\eta}(t)$ satisfies the modal equation of motion:

$$\ddot{\eta}(t)+2\zeta\omega\dot{\eta}(t)+\omega^2\eta(t)=p(t) \tag{6}$$

where $\omega = 2\pi f$ (rad/s) and $p(t)$ is the modal force. The modal force is modelled as a stationary process with a constant PSD of S; and prediction error as independent and identically distributed (i.i.d.) Gaussian white noise with a constant PSD of S_e. The theoretical covariance matrix $\mathbf{E}_k$ then can be written as:

$$\mathbf{E}_k = E[\mathcal{F}_k\mathcal{F}_k^*] = SD_k\boldsymbol{\varphi}\boldsymbol{\varphi}^T + S_e\mathbf{I}_n \tag{7}$$

where

$$D_k = \left[\left(\beta_k^2-1\right)^2+\left(2\zeta\beta_k\right)^2\right]^{-1} \qquad \beta_k = f/\mathrm{f}_k \tag{8}$$

is the dynamic amplification factor and f_k is the FFT frequency abscissa. Using eigenvector representation of $\mathbf{E}_k$, the resulting NLLF can be rewritten as

$$L = (n-1)N_f \ln S_e + \sum_k \ln\left(SD_k + S_e\right) + S_e^{-1}\left(d - \boldsymbol{\varphi}^T\mathbf{A}\boldsymbol{\varphi}\right) \tag{9}$$

where N_f is the number of FFT data in the band;

$$d = \sum_k \mathcal{F}_k^*\mathcal{F}_k \tag{10}$$

$$\mathbf{A} = \sum_k \left(1+S_e/SD_k\right)^{-1}\mathbf{D}_k \tag{11}$$

$$\mathbf{D}_k = \mathcal{F}_k\mathcal{F}_k^* \tag{12}$$

The NLLF in Eq.(9) depends on $\boldsymbol{\varphi}$ through the quadratic term only. Minimising the NLLF with respect to $\boldsymbol{\varphi}$ and subjecting the unit norm constraint $\boldsymbol{\varphi}^T\boldsymbol{\varphi}=1$, it follows that the MPV of the mode shape is the eigenvector of $\mathbf{A}$ with the largest eigenvalue. The NLLF can then be optimised based on the remaining four parameters, which leads to a fast iterative procedure.

Bayesian method for asynchronous data

When the data is asynchronous, it is generally statistically non-sationary. One empirical approach where the modal identification problem is still tractable is to assume the data to be stationary but with imperfect coherence among the modal responses contributing to different data channels [42]. Whether data channels are synchronous is assumed to be known a priori, which is typically the case in real implementation. Define a 'synchronous data group' as a set of data channels that samples the data synchronously (i.e., using the same clock). For example, this can refer to the three data channels from a given tri-axial sensor when it is not synchronised with other sensors; or the data channels from a group of sensors when they are synchronised using the same clock (e.g. GPS).

Let the whole measurement array comprise n_g groups. Let $\mathbf{u}_i \in R^{n_i}$ be the part of the mode shape $\boldsymbol{\varphi}$ measured by the i th group with n_i DOFs; $\ddot{\eta}_{ki} \in C$ and $\boldsymbol{\varepsilon}_{ki} \in C^{n_i}$ be the FFT of the modal acceleration and prediction error associated with the i th group, respectively. The FFT of measured data is now modelled as

$$\mathcal{F}_k = \begin{bmatrix} \mathbf{u}_1 \ddot{\eta}_{k1} \\ \vdots \\ \mathbf{u}_{n_g} \ddot{\eta}_{kn_g} \end{bmatrix} + \begin{bmatrix} \boldsymbol{\varepsilon}_{k1} \\ \vdots \\ \boldsymbol{\varepsilon}_{kn_g} \end{bmatrix} \tag{13}$$

Note that the synchronous case in Eq.(5) corresponds to $\ddot{\eta}_{ki}$ being identically the same for all i.

Assume that all the measured data channels are set to start measuring at the same time with the same measurement duration. Otherwise, the time delay between the synchronous data groups can be compensated using conventional time shift estimation methods [43]. In this context, the asynchronous issue are mainly due to the random time drifts from different sampling clocks. The modal contribution in different synchronous data groups can be assumed as asynchronised realisations of the same modal response. The theoretical covariance matrix $\mathbf{E}_k$ for asynchronous data then can be given by:

$$\mathbf{E}_k = SD_k \begin{bmatrix} \mathbf{u}_1\mathbf{u}_1^T & \chi_{k12}\mathbf{u}_1\mathbf{u}_2^T & \cdots & \chi_{k1n_g}\mathbf{u}_1\mathbf{u}_{n_g}^T \\ \chi_{k21}\mathbf{u}_2\mathbf{u}_1^T & \mathbf{u}_2\mathbf{u}_2^T & & \vdots \\ \vdots & & \ddots & \vdots \\ \chi_{kn_g1}\mathbf{u}_{n_g}\mathbf{u}_1^T & \cdots & \cdots & \mathbf{u}_{n_g}\mathbf{u}_{n_g}^T \end{bmatrix} + \begin{bmatrix} S_{e1}\mathbf{I}_{n_1} & & \\ & \ddots & \\ & & S_{en_g}\mathbf{I}_{n_g} \end{bmatrix} \tag{14}$$

where $\chi_{kij} \in C$ ($|\chi_{kij}| \le 1$) is the coherence between i th and j th group at frequency f_k:

$$\chi_{kij} = \frac{E\left(\ddot{\eta}_{ki}\ddot{\eta}_{kj}^*\right)}{\sqrt{E\left(\ddot{\eta}_{ki}\ddot{\eta}_{ki}^*\right)E\left(\ddot{\eta}_{kj}\ddot{\eta}_{kj}^*\right)}} \tag{15}$$

Based on this model, the modal parameters also include the (complex-valued) coherences among the modal responses of different groups, whose identification turns out to be computationally non-trivial. One simplifying assumption is to set the coherences to be zero, which is justified when the synchronisation degree between groups is low. Together with eigenvector representation of $\mathbf{E}_k$, the resulting NLLF can be rewritten as:

$$L = \sum_{i=1}^{n_g}\left[(n_i - 1)N_f \ln S_{ei} + \sum_k \ln\left(SD_k c_i + S_{ei}\right) + S_{ei}^{-1}\left(d_i - \bar{\mathbf{u}}_i^T \mathbf{A}_i \bar{\mathbf{u}}_i\right)\right] \tag{16}$$

where

$$d_i = \sum_k \mathcal{F}_{ik}^* \mathcal{F}_{ik} \tag{17}$$

$$\mathbf{A}_i = \sum_k \left(1 + S_{ei} / SD_k c_i\right)^{-1} \mathbf{D}_{ik} \tag{18}$$

$$\mathbf{D}_{ik} = \mathcal{F}_{ik}\mathcal{F}_{ik}^* \tag{19}$$

In the above equations, $\mathcal{F}_{ik}$ is the FFT of measured data associated with the i th synchronous group in the selected frequency band; $c_i = \|\mathbf{u}_i\|^2$ and $\bar{\mathbf{u}}_i = \mathbf{u}_i / \|\mathbf{u}_i\|$ so that $\|\bar{\mathbf{u}}_i\| = 1$; S_{ei} is the prediction error PSD of the i th group.

Similar to the mode shape for synchronous data, the MPV of $\bar{\mathbf{u}}_i$ can be obtained as the eigenvector of $\mathbf{A}_i$ with the largest eigenvalue, based on which an iterative procedure can be developed. After the MPV of c_i and $\bar{\mathbf{u}}_i$ have been determined, the MPV of mode shape $\boldsymbol{\varphi}$ can be recovered by

$$\hat{\boldsymbol{\varphi}} = \begin{bmatrix} s_1\sqrt{\hat{c}_1}\hat{\bar{\mathbf{u}}}_1 \\ \vdots \\ s_i\sqrt{\hat{c}_i}\hat{\bar{\mathbf{u}}}_i \\ \vdots \\ s_{n_g}\sqrt{\hat{c}_{n_g}}\hat{\bar{\mathbf{u}}}_{n_g} \end{bmatrix} \tag{20}$$

where a hat '^' denotes MPV; $s_i = \pm 1$ is the relative sign between partial mode shapes $\bar{\mathbf{u}}_i$. As the coherence among synchronous data groups is assumed to be zero, $+\bar{\mathbf{u}}_i$ and $-\bar{\mathbf{u}}_i$ give the same value of NLLF and hence s_i cannot be identified. This is one fundamental limitation of asynchronous data with zero coherence. In practice, s_i can be determined from intuition (e.g., spatial continuity of mode shapes) or an empirical coherence analysis of channels of different groups.

4.2 Mode shape assembly

Using the Bayesian method in Section 4.1, the mode shapes in the individual setups can be identified. It remains to assemble the global mode shape containing all the measured DOFs measured in different setups.

Let $\boldsymbol{\Phi} \in R^{n'}$ be the assembled global mode shape of a mode, where n' is the number of all measured DOFs. Let $\mathbf{L}_i \in R^{n_i' \times n'}$ be a selection matrix such that $\boldsymbol{\varphi}_i = \mathbf{L}_i\boldsymbol{\Phi}$ gives the local mode shape confined to the i th setup, where $n_i'\,(i = 1,...,n_s)$ is the number of measured DOFs in the i th setup and n_s is the number of setups. The (j,k)-entry of $\mathbf{L}_i$ is equal to 1 if DOF k is measured by the j th channel in the i th setup, and zero otherwise. Assuming unit norm for the assembled global mode shape (i.e. $\|\boldsymbol{\Phi}\| = 1$), the mode shape is identified as the one that minimises the following objective function:

$$\begin{aligned} J(\boldsymbol{\Phi}, \gamma; \mathbf{c}, \boldsymbol{\lambda}) = & \sum_{i=1}^{n_s} (\mathbf{L}_i\boldsymbol{\Phi} - c_i\hat{\boldsymbol{\varphi}}_i)^T (\mathbf{L}_i\boldsymbol{\Phi} - c_i\hat{\boldsymbol{\varphi}}_i) \\ & + \gamma(1 - \boldsymbol{\Phi}^T\boldsymbol{\Phi}) + \sum_{i=1}^{n_s} \lambda_i(\boldsymbol{\Phi}^T\mathbf{L}_i^T\mathbf{L}_i\boldsymbol{\Phi} - c_i^2) \end{aligned} \tag{21}$$

where $\hat{\boldsymbol{\varphi}}_i$ is the MPV of mode shape for the i th setup; γ is a Lagrange multiplier that enforces the unit norm constraint of $\boldsymbol{\Phi}$; $\mathbf{c} = \begin{bmatrix} c_1 & \cdots & c_{n_s} \end{bmatrix}$ is the mode shape scaling factors

with the constraints $c_i^2 = \|\boldsymbol{\varphi}_i\|^2 (i = 1,..., n_s)$ enforced by the Lagrange multipliers $\boldsymbol{\lambda} = [\lambda_1,..., \lambda_{n_s}]$.

Direct differentiation of J with respect to c_i yields the optimal value of λ_i and c_i

$$\lambda_i = 1 - \frac{\left|\hat{\boldsymbol{\varphi}}_i^T \boldsymbol{\varphi}_i\right|}{\|\boldsymbol{\varphi}_i\|} \tag{22}$$

$$c_i = \mathrm{sgn}\left(\hat{\boldsymbol{\varphi}}_i^T \boldsymbol{\varphi}_i\right)\|\boldsymbol{\varphi}_i\| \tag{23}$$

where sgn(.) denotes the sign of its argument. On the other hand, setting $\nabla_{\boldsymbol{\Phi}}^T J = \mathbf{0}$ with respect to $\boldsymbol{\Phi}$ gives:

$$\mathbf{B}\boldsymbol{\Phi} + \mathbf{b} = \gamma\boldsymbol{\Phi} \tag{24}$$

where

$$\mathbf{B} = \sum_{i=1}^{n_s} (1 + \lambda_i)\mathbf{L}_i^T\mathbf{L}_i \tag{25}$$

$$\mathbf{b} = -\sum_{i=1}^{n_s} c_i \mathbf{L}_i^T \hat{\boldsymbol{\varphi}}_i \tag{26}$$

Eq.(24) is a 'constrained eigenvalue problem', whose solution can be obtained as the first half of the eigenvectors of $\mathbf{D}$ with the smallest real eigenvalue:

$$\mathbf{D} = \begin{bmatrix} \mathbf{B} & \mathbf{b}\mathbf{b}^T \\ \mathbf{I}_{n'} & \mathbf{B} \end{bmatrix} \tag{27}$$

In this context, the optimal value of $\boldsymbol{\Phi}$ can be obtained given $\{\lambda_i, c_i\}$. Recall that $\{\lambda_i, c_i\}$ can be updated using Eq.(22) and (23) given $\boldsymbol{\Phi}$. This allows an iterative procedure to be developed.

5. Investigation with field data

The modal identification results and their quality based on both synchronous and asynchronous ambient data are addressed in this section. To indicate the modes of interest and the selection of frequency bands, the singular value spectra of the measured data are first examined in Section 5.1. The quality of identified modal parameters based on asynchronous data is then assessed in Section 5.2 by comparing to the synchronous counterparts. Detailed investigation on the quality of assembled global mode shapes using asynchronous data are

addressed in Section 5.3. Identification uncertainties are investigated in Section 5.4. Some comments on the computational time of modal analysis are drawn in Section 5.5.

It should be noted that for the tables and figures in this section that summarise the identification results, the data are referred based on the floor number of the measurement locations for each setup rather than the setup number directly. This is because the same setup number for synchronous and asynchronous data may not refer to the same measurement locations. For example, Setup 5 for asynchronous data refers to the measured locations on 2/F but that for synchronous data refers to 3/F (see details in Section 3.3).

5.1 Data spectra

The root singular value (SV) spectrum, i.e. the square root of eigenvalues of the sample power spectrum density (PSD) matrix, is a conventional tool used in OMA which visualise the potential modes in the frequency domain. It can also indicate potential synchronisation problems between data channels. Figure 5 and Figure 6 show the root SV spectrum of Setup 1 (i.e., 7/F) for synchronous and asynchronous data, respectively. The peaks displaying dynamic amplification in the figures indicate potential modes. The horizontal bars '[-]' and the squares denote the frequency bands (hand-picked which adequately cover the resonance region of the modes of interest) and the initial guesses of natural frequencies used for modal identification (picked at the spectral peaks), respectively. For synchronous data, there is only one line significantly above the remaining ones in each selected frequency band, indicating one mode dominating the band. This is not the case for the root SV spectrum of asynchronous data in Figure 6, however. Multiple peaks can be found in each band, reflecting the number of synchronisation groups (five in this test for asynchronous data).

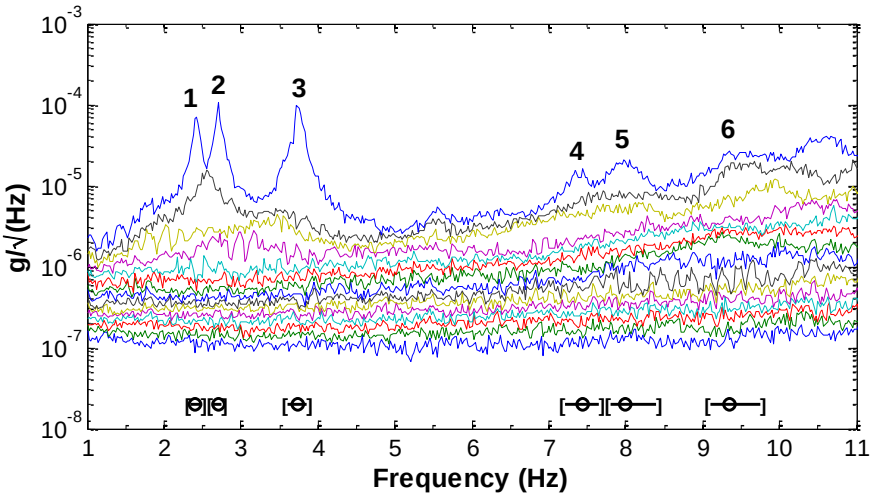

Figure 5. Root Singular Value Spectrum of Setup 1 (7/F), Synchronous Data

In this study, modal identification focuses on the first six modes, which correspond to different situations typically encountered in applications. The peaks of the first three modes are significantly above the remaining lines, indicating high signal-to-noise (s/n) ratios (the ratio of the spectral density of modal excitation to the spectral density of prediction error at the resonance peak, i.e., $S/\left(4\zeta^2 S_e\right)$). The s/n ratios for the fourth and fifth modes are relatively low compared to the first three modes. This is common in real applications when the mode is not well excited or the data is not dominated by structural dynamics. The sixth mode represents the extreme case one may face in field tests where the s/n ratio is very low. Table 1 summarises the sample mean of s/n ratio among the setups for both asynchronous and synchronous data calculated based on the identified modal parameters as a reference. It should be noted that the s/n ratios of the modes between the synchronous and asynchronous data need not be the same as they are measured in different time periods. On the other hand, they are in the same order of magnitude, suggesting no significant environmental variations between these two data. The identified modal parameters between these two data sets are comparable, e.g., their damping ratios (which are often thought to be amplitude-dependent) should refer to similar vibration levels (e.g., serviceability in contrast to damage state levels). However, this does not mean that there is no difference in the numerical values as fundamentally these identification results are determined based on different measured data.

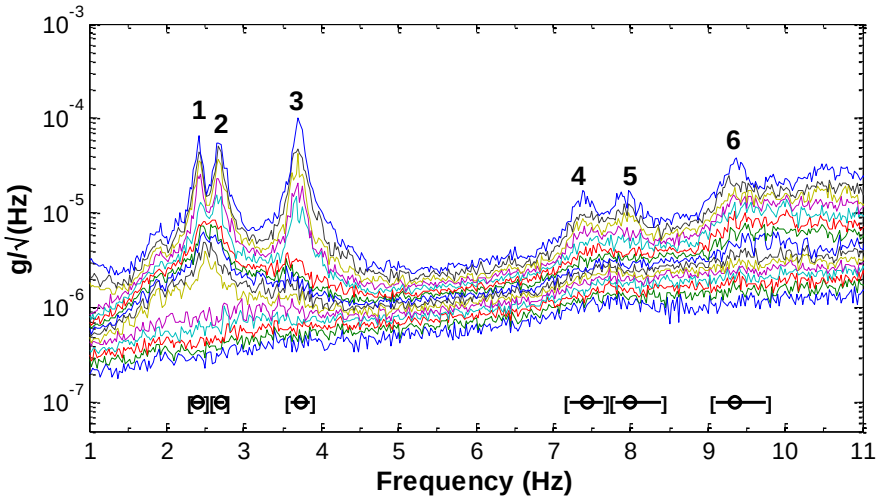

Figure 6. Root Singular Value Spectrum of Setup 1 (7/F), Asynchronous Data

Table 1. Sample Mean of s/n Ratio Among Setups

		Mode					
		1	2	3	4	5	6
Modal s/n Ratio	Asyn.	712	954	5101	36	68	33
	Syn.	1384	1612	3967	32	59	22

5.2 Identified modal properties in different setups

Figure 7 and Figure 8 show the identified natural frequencies and damping ratios among individual setups, respectively. The parameters identified based on asynchronous data are shown with blue circles at the MPVs and the synchronous ones are shown with red squares. The error bars cover +/- 2 posterior standard deviation. It can be seen that the identified natural frequencies and damping ratios based on asynchronous data generally agree well with their synchronous counterparts. Small discrepancies can be found in some setups, e.g., the identified natural frequencies and damping ratios of Mode 5 on 5/F. Besides the environmental variations, this may be also due to the low s/n ratio that affects the identification quality.

The sample mean and c.o.v. (sample standard deviation / sample mean) of the identified modal parameters for both asynchronous and synchronous data among the setups are shown in Table 2 and Table 3, respectively. It can be seen that the sample mean of natural frequencies identified based on asynchronous data are very close to the synchronous

counterparts. The identified values vary among the setups but the variability is so small (less than 1%) that can be ignored for practical purposes. The sample mean of identified damping ratios based on asynchronous data are also close to the ones identified based on synchronous data. Significant variability can be found in the identified root modal force PSD (sample c.o.v. ranges between 20-40%) while this merely reflects the variation of environmental conditions among the setups.

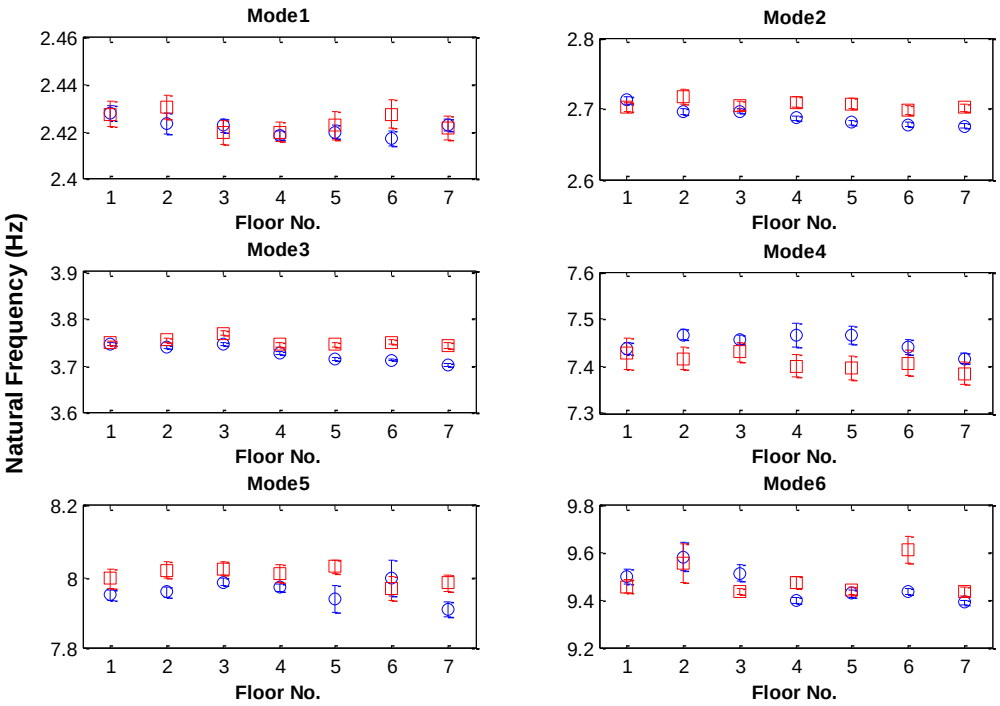

Figure 7. Identification Result (±2 Standard Derivation Error Bar) of Natural Frequencies across different setups; Asynchronous Data: Blue Line with Circle, Synchronous Data: Red Line with Square.

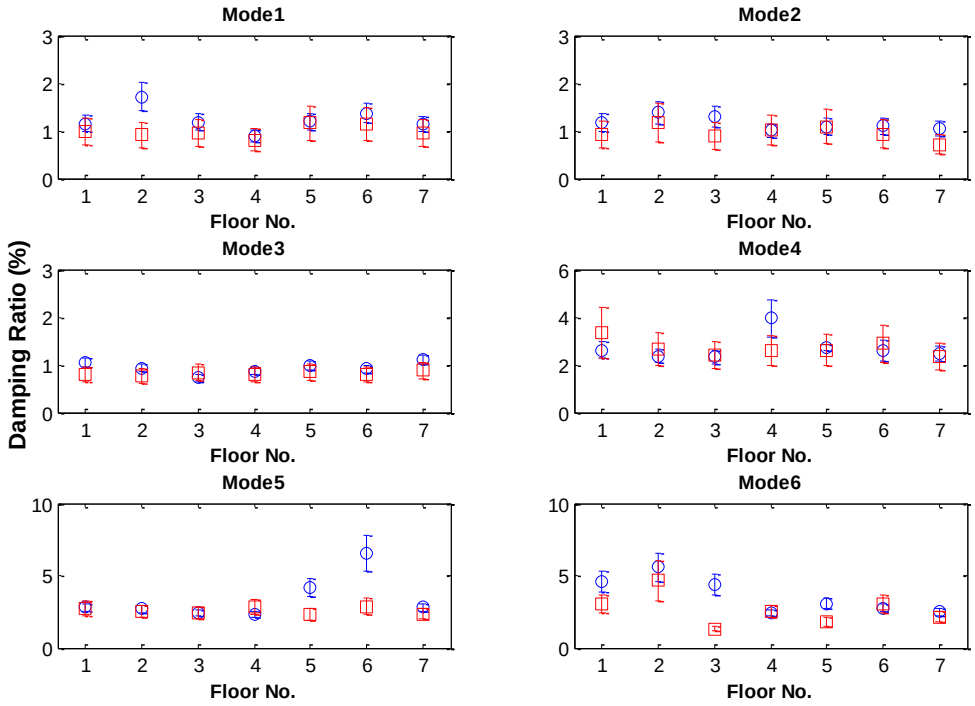

Figure 8. Identification Result (±2 Standard Derivation Error Bar) of Damping Ratio across different setups; Asynchronous Data: Blue Line with Circle, Synchronous Data: Red Line with Square.

Table 2. Sample Mean of Identified Modal Parameters Among Setups

		Mode					
		1	2	3	4	5	6
Natural Frequency (Hz)	Asyn.	2.422	2.689	3.728	7.450	7.959	9.469
	Syn.	2.424	2.705	3.752	7.409	8.005	9.492
Damping Ratio (%)	Asyn.	1.24	1.15	0.94	2.72	3.40	3.62
	Syn.	0.99	0.96	0.82	2.69	2.58	2.65
Root Modal Force PSD ($\mu g/\sqrt{Hz}$)	Asyn.	1.40	1.48	1.56	0.84	1.19	1.76
	Syn.	1.07	1.09	1.00	0.58	0.89	1.16

Table 3. Sample c.o.v. (%) of Identified Modal Parameters Among Setups

		Mode					
		1	2	3	4	5	6
Natural Frequency	Asyn.	0.15	0.48	0.47	0.26	0.37	0.73
	Syn.	0.18	0.23	0.24	0.22	0.29	0.73

Damping Ratio	Asyn.	20	12	14	21	45	34
	Syn.	13	15	5	12	9	41
Root Modal Force PSD	Asyn.	40	28	51	40	18	22
	Syn.	43	33	55	14	27	31

5.3 Identified mode shape

Figure 9 to Figure 14 shows the global mode shapes of the first six modes assembled by the global least square method using the mode shapes identified in individual setups for both synchronous and asynchronous cases. The mean natural frequency and damping ratio among all setups are also shown in the figure with the identification uncertainty in the brackets (see discussion in Section 5.4). The Modal Assurance Criterion (MAC) values between the mode shapes identified based on asynchronous and synchronous data for both individual setup and global assembled cases are listed in Table 4. Mode 1 involves the whole building translating in the x-direction. It can be seen that there is also a slight rotation about the top left of the figure in the plan view which may due to the mass distribution of the whole building. Mode 2 is a translational mode along the y-direction. Little rotation can be found in this mode, which is different from the first mode. Mode 3 is a torsional mode with the torsional centre located at the left side of the T-shape connection. For the first three modes, the assembled mode shape based on asynchronous data is very close to the one based on synchronous data. The MAC values between these two are calculated to be 0.9991, 0.9995 and 0.9980 from Mode 1 to Mode 3, respectively. The identification result based on asynchronous data can provide a good estimation of the global mode shape when the s/n ratio of the mode is high. Mode 4 is the second translational mode in the x-direction. Similar to Mode 1, slight rotation can be found in this mode as well. Mode 5 is the second translational mode in the y-direction. Compared to the first three modes, the s/n ratios for Mode 4 and Mode 5 are not high. Nevertheless, the global mode shapes based on asynchronous data are physically sound. The MAC values between the synchronous and asynchronous data for these two modes are calculated to be 0.9465 and 0.9813, respectively.

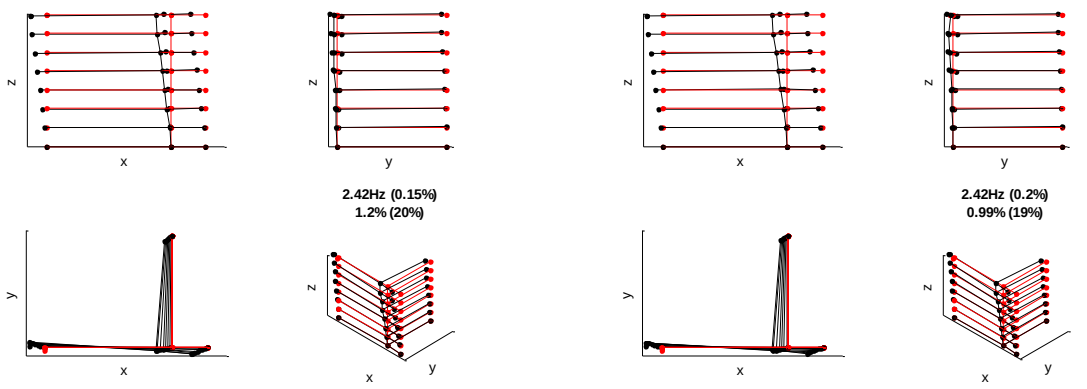

(a) (b)

Figure 9. Mode Shape of Mode 1 (a) Asynchronous Data (b) Synchronous Data

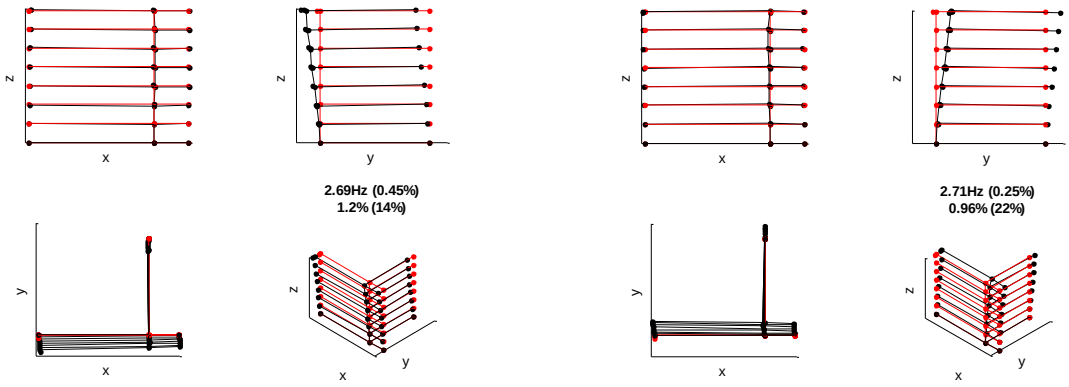

(a) (b)

Figure 10. Mode Shape of Mode 2 (a) Asynchronous Data (b) Synchronous Data

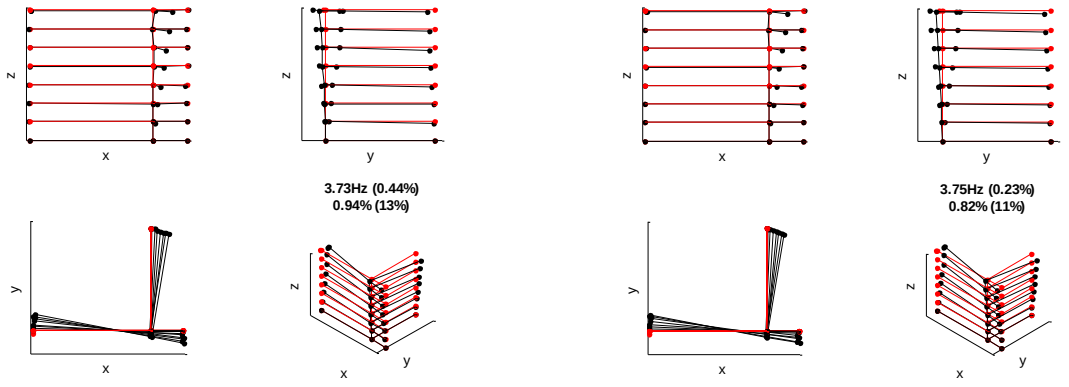

(a) (b)

Figure 11. Mode Shape of Mode 3 (a) Asynchronous Data (b) Synchronous Data

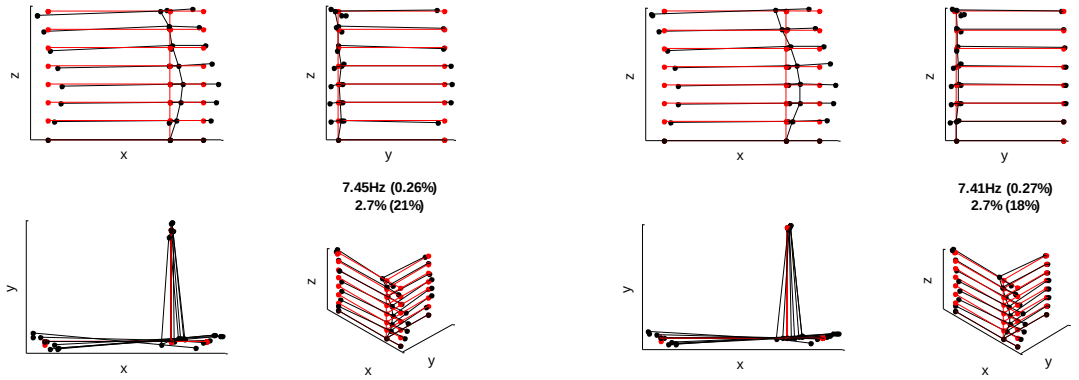

(a) (b)

Figure 12. Mode Shape of Mode 4 (a) Asynchronous Data (b) Synchronous Data

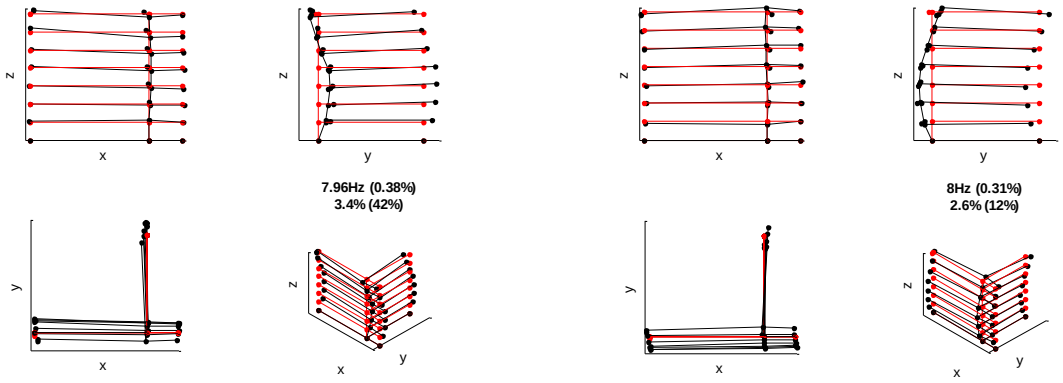

(a) (b)

Figure 13. Mode Shape of Mode 5 (a) Asynchronous Data (b) Synchronous Data

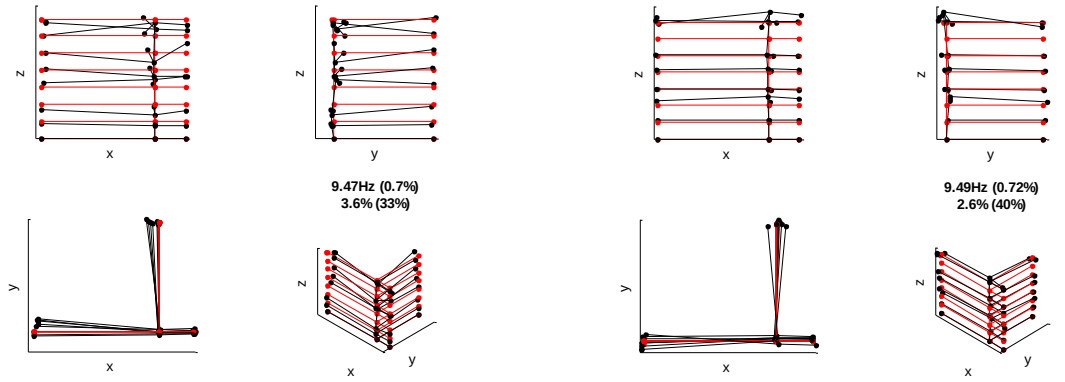

(a) (b)

Figure 14. Mode Shape of Mode 6 (a) Asynchronous Data (b) Synchronous Data

Table 4. Mode Shape MAC values

Floor No.	Mode					
	1	2	3	4	5	6
1/F	0.9999	0.9999	0.9996	0.9143	0.9949	0.9082
2/F	0.9995	0.9998	0.9979	0.9717	0.9857	0.9112
3/F	0.9993	0.9995	0.9979	0.9775	0.9904	0.6904
4/F	0.9994	0.9993	0.9990	0.9642	0.9936	0.7955
5/F	0.9993	0.9996	0.9988	0.8398	0.8709	0.7941
6/F	0.9995	0.9996	0.9995	0.9410	0.8763	0.6583
7/F	0.9991	0.9997	0.9986	0.9637	0.9904	0.8348
Global	0.9991	0.9994	0.9980	0.9465	0.9813	0.0249

Significant discrepancy can be found in the mode shape of Mode 6 where the MAC value between asynchronous and synchronous cases is only 0.02. As shown in Table 4, the MAC values in individual setups are not low (from 0.65 to 0.91) for Mode 6 but it is quite low (0.02) in the assembled global mode shape. Bayesian approach incorporating multiple setups [26] has also been used to check the global mode shape of synchronous data, which shows similar results. This means the errors are not caused by mode shape assembly. Further analysis reveals that this may be due to the erroneous modelling in the z-direction of the measured data. To illustrate this point, Figure 16 and Figure 17 shows the root PSD spectrum of the data channels measured by the reference sensor in Setup 2 (6/F) around Mode 6 for both synchronous and asynchronous data. The PSD spectra for both synchronous and asynchronous suggest that Mode 6 has little resonant component of Mode 6 in the z-direction. The situation is similar for other sensors and setups (details omitted). Hence the identification results do not correctly reflect the actual modal properties of Mode 6, especially the mode shape values in the z-direction. When assembling the global mode shape, the (erroneous) mode shape values in the z-direction of the reference sensor lead to further estimation errors in the relative scaling between partial mode shapes in different setups. In this context, even the identification results based on synchronous data may not provide a reasonable estimation on the global mode shape of Mode 6. To examine whether the vibration data in the vertical direction may have spurious effects on the identification results of Mode 6 (which is predominantly horizontal), additional analysis of Mode 6 has been conducted where the data in the vertical channels are not used. Figure 15 shows the resulting global mode shape of Mode 6. The identified mode shapes between synchronous and asynchronous data are quite close, with a MAC value of 0.978. The identified mode shapes in the horizontal directions based on asynchronous data are quite close to their synchronous counterparts. The results

suggest that the issue is associated with the modelling error in the z-direction of measured data (especially for the reference locations).

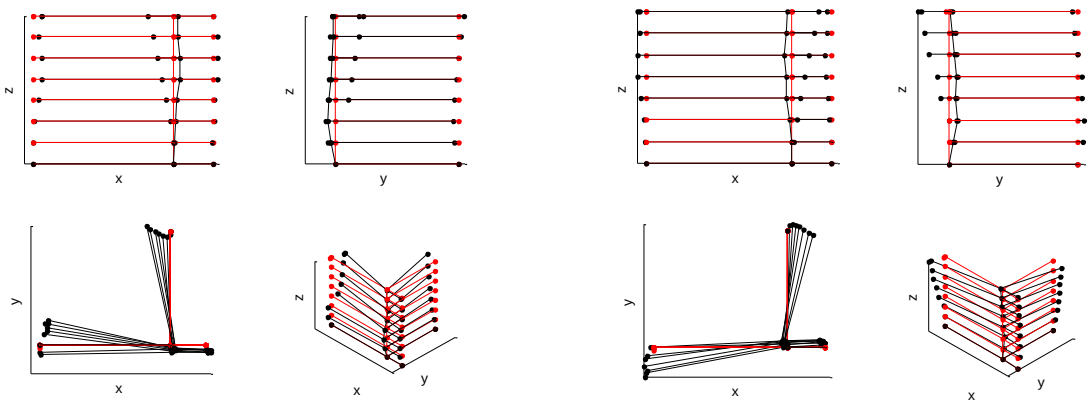

(a) (b)

Figure 15. Mode Shape of Mode 6 (horizontal channels only) (a) Asynchronous Data (b) Synchronous Data

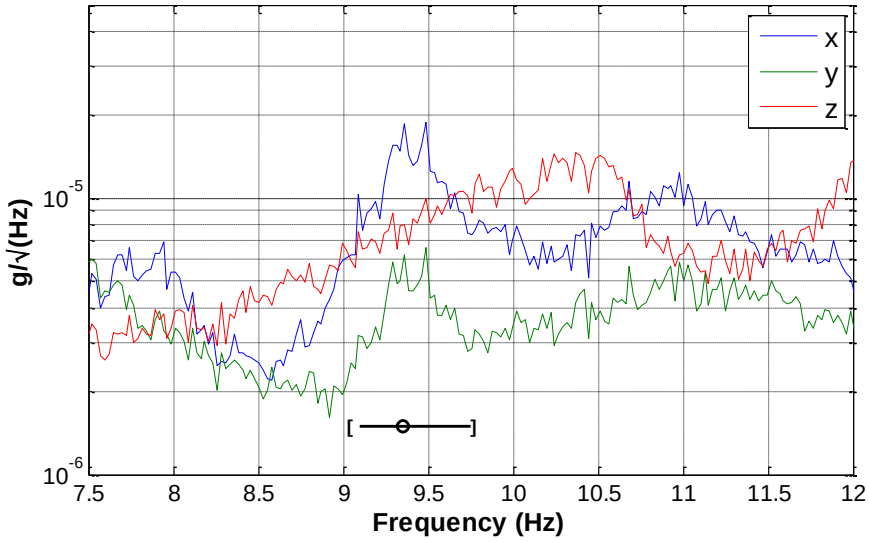

Figure 16. Root PSD Spectrum of Setup 2 (6/F), Asynchronous Data

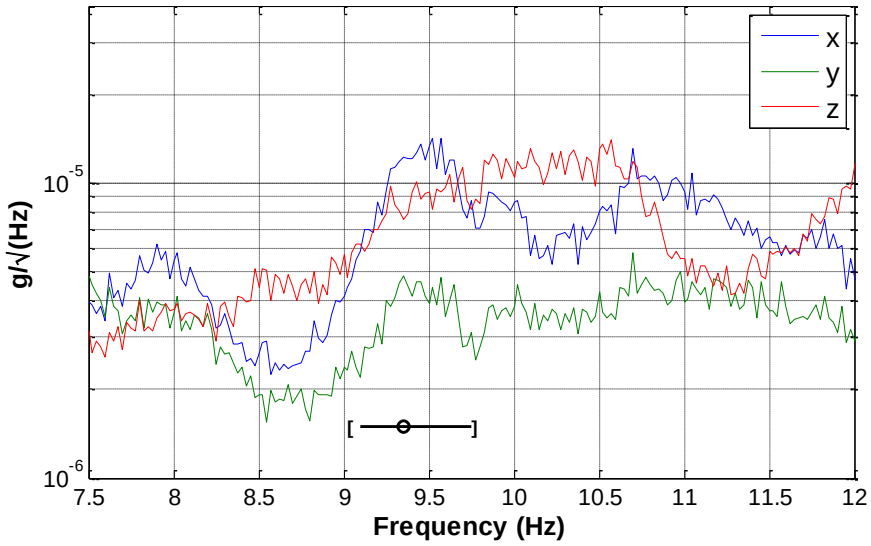

Figure 17. Root PSD Spectrum of Setup 2 (6/F), Synchronous Data

5.4 Identification uncertainty

Table 5 to Table 7 list the posterior c.o.v. values of natural frequencies, damping ratios and mode shapes in the seven setups for both synchronous and asynchronous cases, respectively. It can be seen that the posterior c.o.v. of natural frequencies are small (less than 1%) while the posterior c.o.v.s of damping ratios are much higher. Compared with those of synchronous data, the posterior c.o.v.s of asynchronous data are of similar order. For the identified mode shape, the posterior c.o.v.s for asynchronous data are larger than the synchronous counterparts, especially the first three modes. This is reasonable as the mode shape for asynchronous data are partially identified within each synchronous group hence intuitively less data is used for inference.

It should be noted that the posterior c.o.v. here reflects the unresolved uncertainty of a modal parameter given measured data and model assumptions in a particular setup. It does not imply how close the identified results are to the 'true' values due to the presence of modelling error. The posterior uncertainty of synchronous and asynchronous data cannot be directly compared as they are obtained based on different identification model and different data (as they are measured in different time periods).

On the other hand, the posterior c.o.v. in this section is different from the sample c.o.v. discussed in Section 5.3. The latter merely reflects the statistical variability of the MPV among the setups. The identification uncertainty shown in the mode shape figures are

representative values which can be calculated as the sum of sample c.o.v. and sample mean of posterior c.o.v..

Table 5. Posterior c.o.v. of Natural Frequencies (%)

Mode		Floor No.							Mean
		1/F	2/F	3/F	4/F	5/F	6/F	7/F	
1	Asyn.	0.06	0.09	0.06	0.04	0.06	0.06	0.06	0.06
	Syn.	0.11	0.11	0.10	0.09	0.12	0.13	0.10	0.11
2	Asyn.	0.08	0.07	0.07	0.05	0.05	0.05	0.05	0.06
	Syn.	0.11	0.20	0.11	0.14	0.14	0.10	0.08	0.13
3	Asyn.	0.04	0.03	0.03	0.03	0.03	0.03	0.04	0.03
	Syn.	0.06	0.06	0.07	0.06	0.07	0.06	0.07	0.07
4	Asyn.	0.08	0.07	0.07	0.16	0.13	0.10	0.07	0.10
	Syn.	0.22	0.16	0.14	0.16	0.17	0.19	0.15	0.17
5	Asyn.	0.10	0.10	0.07	0.07	0.24	0.31	0.13	0.15
	Syn.	0.16	0.13	0.12	0.16	0.12	0.21	0.14	0.15
6	Asyn.	0.16	0.31	0.18	0.07	0.08	0.07	0.06	0.13
	Syn.	0.15	0.43	0.07	0.13	0.09	0.29	0.10	0.18

Table 6. Posterior c.o.v. of Damping Ratio (%)

Mode		Floor No.							Mean
		1/F	2/F	3/F	4/F	5/F	6/F	7/F	
1	Asyn.	8	8	7	7	7	7	7	7
	Syn.	15	14	15	14	15	15	15	15
2	Asyn.	8	9	8	7	8	8	7	8
	Syn.	16	17	16	16	17	16	15	16
3	Asyn.	5	5	5	4	4	4	4	5
	Syn.	10	10	10	10	10	10	10	10
4	Asyn.	7	6	6	10	2	8	6	6
	Syn.	16	13	12	12	13	14	12	13
5	Asyn.	4	5	4	4	8	10	5	6
	Syn.	9	8	8	9	8	10	8	9
6	Asyn.	8	9	9	5	6	5	4	6
	Syn.	10	15	7	9	8	10	8	10

Table 7. Posterior c.o.v. of Mode Shape (%)

Mode		Floor No.							Mean
		1/F	2/F	3/F	4/F	5/F	6/F	7/F	
1	Asyn.	1.66	2.72	3.36	3.65	3.89	3.85	3.85	3.28
	Syn.	0.87	0.88	0.94	0.83	0.88	0.89	0.84	0.88
2	Asyn.	1.68	2.59	3.32	3.78	3.91	3.99	4.04	3.33
	Syn.	0.66	1.01	0.69	0.86	0.86	0.95	0.83	0.84

3	Asyn.	0.92	1.72	2.04	2.40	2.50	2.53	2.52	2.09
	Syn.	0.59	0.73	0.34	0.38	0.45	0.41	0.37	0.47
4	Asyn.	3.04	3.09	2.84	3.04	18.50	3.65	2.92	5.30
	Syn.	2.51	2.70	2.32	2.16	2.38	2.58	2.50	2.45
5	Asyn.	2.04	2.51	2.30	2.04	3.94	2.58	2.46	2.55
	Syn.	1.32	1.38	1.30	1.59	2.27	3.02	1.81	1.81
6	Asyn.	2.51	2.49	3.28	2.93	2.99	2.52	2.39	2.73
	Syn.	2.41	2.48	2.92	2.78	3.00	3.47	2.79	2.83

5.5 Computational time

Computational efficiency is an important factor that should be taken into consideration when assessing the significance of using asynchronous data in OMA. For reference, some comments regarding the computational time for modal identification are drawn in this section. The analysis in this work was performed using MATLAB R2014a on an HP Compaq 800 G1 Elite Desktop (Intel Core i5, 2GHz and 8GB of RAM). The optimization of the NLLF function was conducted via the MATLAB function `fminsearch` and the convergence tolerance of the iteration procedure is set to be 10^{-6} on a fractional basis for all parameters.

Table 8 summarises the computational time of MPV and posterior uncertainty for the modes analysed in this work. It can be seen that asynchronous data requires more time for determining the MPV than synchronous data, especially for the last three modes where the s/n ratio is low. For posterior c.o.v., the computational time used for asynchronous data is slightly less than the one for synchronous data. It should be noted that the computational time increases with number of setups (which is seven in this work). Nevertheless, for asynchronous data it generally requires a few minutes for the whole computational process, which is still quite feasible to be implemented even on site.

Table 8. Computational Time (sum of the required time for all the setups)

Mode		Time required (s)	
		MPV	Posterior c.o.v.
1	Asyn.	27	3
	Syn.	8	7
2	Asyn.	32	2
	Syn.	10	7
3	Asyn.	31	5
	Syn.	11	10
4	Asyn.	300	9
	Syn.	59	14
5	Asyn.	394	13

	Syn.	36	17
6	Asyn.	479	15
	Syn.	54	19

6. Conclusions

This paper has investigated the quality of modal identification results using asynchronous ambient data with multiple setups in full-scale tests. An eight-storey office building has been used as a vehicle for investigation. Operational modal analysis has been conducted and the quality of modal identification results has been investigated comparing to the ones identified based on synchronous data. The posterior uncertainty of the identified modal parameters has also been discussed.

The study reveals that the identified natural frequencies and damping ratios identified based on asynchronous data are close to their synchronous counterparts. For modes with high modal s/n ratio, the assembled global mode shapes based on asynchronous data are practically the same with the ones based on synchronous data. Challenging situations exist when the modes may have high modelling error and low s/n ratio. The identification errors in the mode shapes of individual setups smear into the assembled mode shape in a non-trivial manner. In this context, neither the synchronous data nor asynchronous data can provide a good estimation on the global mode shape. The identification uncertainty has also been investigated. The mode shapes identified based on asynchronous data generally have larger uncertainty than those based on synchronous data as less information is used for inference. Modal analysis based on asynchronous data generally takes more time than that of synchronous data. However, it is still feasible to be conducted on site as the whole computational process can be done in several minutes.

The global least square method is used in this work to assemble the global mode shape where the identification results in individual setups are equally weighted regardless of identification quality. Future development of Bayesian methods for asynchronous data is demanded that is capable of incorporating the data in different setups together with probability logic, in which case better estimation of the global mode shape is expected.

Acknowledgements

This paper is based on work funded by UK Engineering & Physical Sciences Research Council (EP/N017897/1). The first and second author would like to acknowledge financial supports by the Tung's scholarship and the China Scholarship Council, respectively.

References

[1] Chang PC, Flatau A, Liu SC. Review Paper: Health Monitoring of Civil Infrastructure. Struct Heal Monit 2003;2:257–67. doi:10.1177/1475921703036169.

[2] Farrar CR, Worden K. An introduction to structural health monitoring. Philos Trans A Math Phys Eng Sci 2007;365:303–15. doi:10.1098/rsta.2006.1928.

[3] Brownjohn JMW. Structural health monitoring of civil infrastructure. Philos Trans A Math Phys Eng Sci 2007;365:589–622. doi:10.1098/rsta.2006.1925.

[4] Sohn H, Farrar CR, Hemez F, Czarnecki J. A Review of Structural Health Monitoring Literature 1996 – 2001. Third World Conf Struct Control 2002:1–7.

[5] Salawu OS. Detection of structural damage through changes in frequency: a review. Eng Struct 1997;19:718–23. doi:10.1016/S0141-0296(96)00149-6.

[6] Hearn G, Testa R. Modal analysis for damage detection in structures. J Struct Eng 1991;117:3042–63.

[7] Brincker R, Ventura CE. Introduction to Operational Modal Analysis. London: Wiley; 2015. doi:10.1002/9781118535141.

[8] Costa BJA, Magalhães F, Cunha Á, Figueiras J. Rehabilitation assessment of a centenary steel bridge based on modal analysis. Eng Struct 2013;56:260–72. doi:10.1016/j.engstruct.2013.05.010.

[9] Li QS, Xiao YQ, Wong CK, Jeary AP. Field measurements of typhoon effects on a super tall building. Eng Struct 2004;26:233–44. doi:10.1016/j.engstruct.2003.09.013.

[10] Wenzel H, Pichler D. Ambient vibration monitoring. Wiley, UK; 2005.

[11] Hermans L, Van Der Auweraer H. Modal Testing and Analysis of Structures Under Operational Conditions: Industrial Applications. Mech Syst Signal Process

1999;13:193–216. doi:10.1006/mssp.1998.1211.

[12] Catbas FN, Kijewski-Correa T, Aktan AE. Structural identification (St-Id) of constructed facilities: Approaches, methods and technologies for effective practice of St-Id. Am Soc Civ Eng, 2011.

[13] Papadimitriou C, Papadioti DC. Component mode synthesis techniques for finite element model updating. Comput Struct 2013;126:15–28. doi:10.1016/j.compstruc.2012.10.018.

[14] Au S-K, Zhang F-L. Fundamental two-stage formulation for Bayesian system identification, Part I: General theory. Mech Syst Signal Process 2015:1–12. doi:10.1016/j.ymssp.2015.04.025.

[15] Ramos LF, Marques L, Lourenço PB, De Roeck G, Campos-Costa A, Roque J. Monitoring historical masonry structures with operational modal analysis: Two case studies. Mech Syst Signal Process 2010;24:1291–305. doi:10.1016/j.ymssp.2010.01.011.

[16] Gentile C, Saisi A. Ambient vibration testing of historic masonry towers for structural identification and damage assessment. Constr Build Mater 2007;21:1311–21. doi:10.1016/j.conbuildmat.2006.01.007.

[17] Brownjohn JMW, Moyo P, Omenzetter P, Lu Y. Assessment of highway bridge upgrading by dynamic testing and finite-element model updating. J Bridg Eng 2003;8:162–72. doi:10.1061/(ASCE)1084-0702(2003)8:3(162).

[18] Brownjohn JMW, Magalhaes F, Caetano E, Cunha A. Ambient vibration re-testing and operational modal analysis of the Humber Bridge. Eng Struct 2010;32:2003–18. doi:10.1016/j.engstruct.2010.02.034.

[19] Lam H-F, Zhang F-L, Ni Y-C, Hu J. Operational modal identification of a boat-shaped building by a Bayesian approach. Eng Struct 2017;138:381–93. doi:10.1016/j.engstruct.2017.02.003.

[20] Ni YC, Lu XL, Lu WS. Field dynamic test and Bayesian modal identification of a special structure - The Palms Together Dagoba. Struct Control Heal Monit 2016;23:838–56. doi:10.1002/stc.1816.

[21] Ni Y, Lu X, Lu W. Operational modal analysis of a high-rise multi-function building with dampers by a Bayesian approach. Mech Syst Signal Process 2017;86:286–307. doi:10.1016/j.ymssp.2016.10.009.

[22] Zhang FL, Xiong HB, Shi WX, Ou X. Structural health monitoring of Shanghai Tower during different stages using a Bayesian approach. Struct Control Heal Monit 2016;23:1366–84. doi:10.1002/stc.1840.

[23] Au S-K. Assembling mode shapes by least squares. Mech Syst Signal Process 2011;25:163–79. doi:10.1016/j.ymssp.2010.08.002.

[24] Reynders, Edwin and Magalhaes, Filipe and Roeck, GD and Cunha A. Merging Strategies for Multi-Setup Operational Modal Analysis: Application to the Luiz I steel Arch Bridge. Proc. IMAC 27, Int. Modal Anal. Conf., 2009.

[25] Döhler M, Lam XB, Mevel L. Uncertainty quantification for modal parameters from stochastic subspace identification on multi-setup measurements. Mech Syst Signal Process 2013;36:562–81. doi:10.1016/j.ymssp.2012.11.011.

[26] Au S-K, Zhang F-L. Fast Bayesian ambient modal identification incorporating multiple setups. J Eng Mech 2012:800–15. doi:10.1061/(ASCE)EM.1943-7889.0000385.

[27] Lam H-F, Hu J, Yang J-H. Bayesian operational modal analysis and Markov chain Monte Carlo-based model updating of a factory building. Eng Struct 2017;132:314–36. doi:10.1016/j.engstruct.2016.11.048.

[28] Zhang F, Ni Y, Lam H. Bayesian structural model updating using ambient vibration data collected by multiple setups. Struct Control Heal Monit 2017.

[29] Mills DL. Internet time synchronization: the network time protocol. IEEE Trans Commun 1991;39:1482–93. doi:10.1109/26.103043.

[30] Kaplan E, Hegarty C. Understanding GPS: principles and applications. Artech house; 2005.

[31] Lynch JP. A Summary Review of Wireless Sensors and Sensor Networks for Structural Health Monitoring. Shock Vib Dig 2006;38:91–128. doi:10.1177/0583102406061499.

[32] Lei Y, Kiremidjian AS, Nair KK, Lynch JP, Law KH. Algorithms for time synchronization of wireless structural monitoring sensors. Earthq Eng Struct Dyn 2005;34:555–73. doi:10.1002/eqe.432.

[33] Elson J, Girod L, Estrin D. Fine-grained network time synchronization using reference broadcasts. ACM SIGOPS Oper Syst Rev 2002;36:147–63. doi:10.1145/844128.844143.

[34] Au S-K. Fast Bayesian FFT method for ambient modal identification with separated modes. J Eng Mech 2011. doi:10.1061/(ASCE)EM.1943-7889.0000213.

[35] Zhu Y-C, Au S-K. Bayesian Operational Modal Analysis with Asynchronous Data, Part I: Most Probable Value. Mech Syst Signal Process 2018;98C:652–66.

[36] Zhu Y-C, Au S-K. Bayesian Operational Modal Analysis with Asynchronous Data, Part II: Posterior Uncertainty. Mech Syst Signal Process 2018;98C:920–35.

[37] Yuen KV, Katafygiotis LS. Bayesian fast Fourier transform approach for modal updating using ambient data. Adv Struct Eng 2003;6:81–95.

[38] Au S-K, Zhang F-L, Ni Y-C. Bayesian operational modal analysis: Theory, computation, practice. Comput Struct 2013;126:3–14. doi:10.1016/j.compstruc.2012.12.015.

[39] Brillinger DR. Time series: data analysis and theory. vol. 36. Siam; 1981.

[40] Beck JL, Katafygiotis LS. Updating Models and Their Uncertainties. I: Bayesian Statistical Framework. J Eng Mech 1998;124:455–61. doi:10.1061/(ASCE)0733-9399(1998)124:4(455).

[41] Au S-K, Zhang F-L. On assessing the posterior mode shape uncertainty in ambient modal identification. Probabilistic Eng Mech 2011;26:427–34. doi:10.1016/j.probengmech.2010.11.009.

[42] Zhu Y-C, Au S-K. Spectral characteristics of asynchronous data in operational modal analysis. Struct Control Heal Monit 2017:e1981. doi:10.1002/stc.1981.

[43] Bjorklund S, Ljung L. A review of time-delay estimation techniques. Decis. Control. 2003. Proc. …, 2003, p. 2502–7.